Manuscript prepared for Earth Syst. Dynam.
with version 3.2 of the LaTeX class copernicus.cls.
Date: 7 February 2011

Climate change under a scenario near 1.5°C of global warming: Monsoon intensification, ocean warming and steric sea level rise

Jacob Schewe[1,2], **Anders Levermann**[1,2], **and Malte Meinshausen**[1]

[1]Earth System Analysis, Potsdam Institute for Climate Impact Research, Potsdam, Germany
[2]Physics Institute, Potsdam University, Potsdam, Germany

Abstract. We present climatic consequences of the Representative Concentration Pathways (RCPs) using the coupled climate model CLIM*BER*-3α, which contains a statistical-dynamical atmosphere and a three-dimensional ocean model. We compare those with emulations of 19 state-of-the-art atmosphere-ocean general circulation models (AOGCM) using MAGICC6. The RCPs are designed as standard scenarios for the forthcoming IPCC Fifth Assessment Report to span the full range of future greenhouse gas (GHG) concentrations pathways currently discussed. The lowest of the RCP scenarios, RCP3-PD, is projected in CLIM*BER*-3α to imply a maximal warming by the middle of the 21st century slightly above 1.5°C and a slow decline of temperatures thereafter, approaching today's level by 2500. We identify two mechanisms that slow down global cooling after GHG concentrations peak: The known inertia induced by mixing-related oceanic heat uptake; and a change in oceanic convection that enhances ocean heat loss in high latitudes, reducing the surface cooling rate by almost 50%. Steric sea level rise under the RCP3-PD scenario continues for 200 years after the peak in surface air temperatures, stabilizing around 2250 at 30 cm. This contrasts with around 1.3 m of steric sea level rise by 2250, and 2 m by 2500, under the highest scenario, RCP8.5. Maximum oceanic warming at intermediate depth (300-800 m) is found to exceed that of the sea surface by the second half of the 21st century under RCP3-PD. This intermediate-depth warming persists for centuries even after surface temperatures have returned to present-day values, with potential consequences for marine ecosystems, oceanic methane hydrates, and ice-shelf stability. Due to an enhanced land-ocean temperature contrast, all scenarios yield an intensification of monsoon rainfall under global warming.

Correspondence to: J. Schewe
(jacob.schewe@pik-potsdam.de)

1 Introduction

In December 2010, the international community agreed, under the United Nations Framework Convention on Climate Change, to limit global warming to below 2°C (*Cancún Agreements*, see http://unfccc.int/files/meetings/cop_16/application/pdf/cop16_lca.pdf). At the same time, it was agreed that a review, to be concluded by 2015, should look into a potential tightening of this target to 1.5°C – in part because climate change impacts associated with 2°C are considered to exceed tolerable limits for some regions, e.g. Small Island States. So far, research into climate system dynamics under strong mitigation scenarios that keep warming below 2°C or even 1.5°C has been sparse. Individual AOGCMs were run for scenarios stabilizing at 2°C (May, 2008) or below (Washington et al., 2009), or for idealized CO_2 rampdown experiments (Wu et al., 2010).

Here we investigate climate projections for the full range of Representative Concentration Pathways (RCPs; Moss et al., 2010) but focus in particular on the lowest scenario RCP3-PD, which reflects a scenario that will peak global mean temperatures slightly above, but close to, 1.5°C above pre–industrial levels in our model. The RCPs were recently developed in order to complement, and in part replace, the Special Report on Emissions Scenarios (SRES; Nakicenovic and Swart, 2000) scenarios, and will be used in the Climate Model Intercomparison Project's Phase 5 (CMIP5) that is to be assessed in the forthcoming Intergovernmental Panel on Climate Change (IPCC) Fifth Assessment Report (AR5). The RCP3-PD scenario is characterized by a peak of atmospheric greenhouse gas (GHG) concentrations in 2040 and a subsequent decline in GHG abundance. After 2070, CO_2 emissions turn negative and remain at around -1 Gt CO_2-eq/yr after 2100 (Meinshausen et al., submitted). Concentrations in the medium-low RCP4.5 and the medium-high RCP6 stabilize by 2150, while concentrations in the high RCP8.5 continue to rise until 2250.

In Section 2, we describe the models and their experimental setup for this study. Simulation results are presented in Section 3, in particular for global mean temperature (3.1), and changes in large scale climate components like oceanic meridional overturning circulation (3.2), monsoon (3.3), global sea level (3.4), and deep ocean temperature (3.5). In Section 4 we provide the physical mechanisms responsible for an asymmetrically slower cooling than warming under RCP3-PD. Section 5 concludes.

2 Models and experiments

Our primary model for investigating key large-scale aspects of climate change under the RCP scenarios is the Earth system model of intermediate complexity CLIM*BER*-3α (Montoya et al., 2005). CLIM*BER*-3α combines a statistical-dynamical atmosphere model (Petoukhov et al., 2000) with a three-dimensional ocean general circulation model based on the GFDL MOM-3 code (Pacanowski and Griffies, 1999) and a dynamic and thermodynamic sea-ice model (Fichefet and Maqueda, 1997). In this study, CLIM*BER*-3α is used without a carbon cycle. The atmosphere model has a coarse horizontal resolution of 22.5° in longitude and 7.5° in latitude, and employs parameterized vertical temperature and humidity profiles. Oceanic wind stress anomalies are computed with respect to the control simulation and added to the climatology of Trenberth et al. (1989). The oceanic horizontal resolution is $3.75° \times 3.75°$ with 24 variably spaced vertical levels. The model's sensitivity to vertical diffusivity (Mignot et al., 2006) and wind stress forcing (Schewe and Levermann, 2010) has been investigated as well as the model's behaviour under glacial boundary conditions (Montoya and Levermann, 2008) and global warming (Levermann et al., 2007). When compared to AOGCMs of the third Coupled Model Intercomparison Project (CMIP3) and previous generations, the model shows qualitatively and quantitatively similar results with respect to large-scale quantities (Gregory et al., 2005; Stouffer et al., 2006b). The model version used here features a low background value of oceanic vertical diffusivity ($0.3 \cdot 10^{-4}$ m^2/s) and an improved representation of the Indonesian throughflow as compared to the version described by Montoya et al. (2005).

We complement our CLIM*BER*-3α projections of global mean temperature with emulations of 19 AOGCMs used in the IPCC Fourth Assessment Report (AR4). These emulations were performed with MAGICC6, a reduced complexity model with an upwelling-diffusion ocean which has been used in the past three IPCC assessment reports (Wigley and Raper, 2001). MAGICC6 was shown to be able to closely emulate the global and hemispheric mean temperature evolution of AOGCMs (Meinshausen et al., 2008). Our AOGCM emulations use RCPs harmonized emission inputs with default efficacies for the individual forcing agents, identical to the model's setup for creating the default RCP GHG concentration recommendations for CMIP5 (Meinshausen et al., submitted). The only exception is that MAGICC6's climate model is calibrated and run for the range of 19 individual AOGCMs, rather than a single median set of climate module parameters.

Our CLIM*BER*-3α experiments focus on the four new RCPs, namely RCP3-PD (van Vuuren et al., 2007), RCP4.5 (Clarke et al., 2007; Smith and Wigley, 2006; Wise et al., 2009), RCP6 (Fujino et al., 2006), and RCP8.5 (Riahi et al., 2007). We use the historical, 21st century and long-term (until 2500) RCP forcing trajectories as provided on http://www.pik-potsdam.de/~mmalte/rcps/ and described in Meinshausen et al. (submitted). These forcings arose from the process of harmonizing RCP emissions, and producing a single default set of GHG concentrations, which are the basis for the CMIP5 intercomparison runs that extend from pre–industrial times to 2300 (CMIP5, http://cmip-pcmdi.llnl.gov/cmip5/forcing.html). The extension beyond 2300 follows the same guiding principle as the extension up to 2300, i.e. a continuation of constant emissions for the RCP3-PD scenario (and correspondingly dropping forcing levels) and a stabilization of GHG concentrations and forcing levels for the upper three RCPs, RCP4.5, RCP6 and RCP8.5.

For being used in CLIM*BER*-3α, we group our forcings on a forcing-equivalence basis, i.e. we aggregate longwave absorbers into a CO_2-equivalence concentration (Fig. 1a and d). The radiative forcing of agents that scatter or absorb shortwave radiation is aggregated and assumed to modulate the incoming solar irradiance, taking into account geometry and albedo (Fig. 1b and e). CLIM*BER*-3α's climate sensitivity is about 3.4°C, which is higher than the average climate sensitivity of the transient AOGCM emulations of 2.9°C (Meinshausen et al., 2008, Table 4), very close to the average of the slab–ocean GCMs of 3.26°C and still close to the IPCC AR4 best estimate of 3°C (Meehl et al., 2007a, Box 10.2). The transient climate response is about 1.9°C for CLIM*BER*-3α, compared to about 1.8°C for the average of IPCC AR4 AOGCMs (Meehl et al., 2007b, Table 8.2).

3 Results

3.1 Global mean temperature

Global mean surface air temperatures, normalized to the period 1980-1999, are shown in Fig. 1c and f relative to pre–industrial (1860-1890) using the median observed temperature increase of 0.52°C (Brohan et al., 2006). The warming projected by CLIM*BER*-3α lies well within the emulation of the AOGCMs (Fig. 1c and f). For the highest scenario, RCP8.5, the simulation yields a temperature increase of up to 8.5°C, while the lowest scenario, RCP3-PD, reaches up to 1.6°C of global warming compared to pre–industrial and then drops at an average rate of about -0.16°C per century. This is about ten times slower than the currently observed

temperature rise of 0.16 to 0.18°C per decade (Trenberth et al., 2007, section 3.4). Although the reduction in GHG concentrations in the RCP3-PD is generally slower than the increase before the peak, this explains only part of the warming/cooling asymmetry: The average cooling rate during the first 100 years after the peak is 12% of the warming rate in the 100 years before the peak; over the same period, the GHG reduction rate is 35% of the increase rate prior to the peak. The mechanisms responsible for this asymmetry will be discussed in Section 4.

3.2 Spatial warming pattern and oceanic overturning

The spatial distribution of temperature change in 2100 reflects the pattern of polar amplification (Winton, 2006), i.e. above-average surface warming in high latitudes (Fig. 2). In the low RCP3-PD scenario (Fig. 2a), warming in the northern North Atlantic region is offset by the cooling effect of a 20% reduction of the Atlantic meridional overturning circulation (AMOC; Fig. 3a) and the associated reduction in oceanic convection and heat release (compare Sec. 4). As the AMOC recovers over the course of the 22nd and 23rd century, this offsetting effect will disappear. In the RCP8.5 scenario (Fig. 2b), the AMOC reduction is relatively smaller compared to the warming, and has no large offsetting effect. The recovery of the AMOC beyond 2200 is facilitated by the retreat of sea ice cover in the North Atlantic (Levermann et al., 2007), which in the case of RCP3-PD even leaves the AMOC stronger in the long-term than under pre–industrial conditions. The behaviour of the AMOC under global warming in CLIM*BER*-3α is a robust feature of most CMIP3 AOGCMs (Gregory et al., 2005), and the mechanisms at play are in qualitative agreement across the models (Levermann et al., 2007). Quantitatively, AOGCMs differ significantly in their response. With respect to the pre–industrial overturning strength, CLIM*BER*-3α is comparable to the IPCC AR4 model average and consistent with observations (cf. Fig. 10.15 in Meehl et al., 2007a). AMOC changes in response to global warming in CLIM*BER*-3α are dominated by changes in heat flux, as in most other CMIP3 models, while hydrological changes tend to have a minor, strengthening effect (Gregory et al., 2005). Further possible AMOC reduction due to Greenland ice sheet melting is not accounted for in these simulations.

3.3 Monsoon intensification

Directly influenced by atmospheric temperature patterns, large-scale monsoon circulations are arguably among the most societally relevant atmospheric systems. Within the limitations of the statistical-dynamical atmosphere model and its coarse resolution, CLIM*BER*-3α simulates the principal patterns of monsoon dynamics and precipitation reasonably well (Fig. 4a), and its seasonal rainfall cycle compares favourably with reanalysis data (Fig. 4b) and IPCC AR4 models (cf. Kripalani et al., 2007, Fig. 1). We find that average monsoon rainfall in Asia and Africa intensifies under global warming (Fig. 5), consistent with many studies using more complex models (e.g. Kripalani et al., 2007). Seasonal (June-August, JJA) mean rainfall associated with the South Asian summer monsoon (including India and the Bay of Bengal) strengthens by 10% (RCP3-PD) to 20% (RCP8.5) until the middle of the 21st century and, for RCP8.5, by up to 30% during the 22nd century (Fig. 5a). Similar results are found for the East Asian (including China, Fig. 5b) and West African (Fig. 5c) monsoon, which both increase by up to 50% for RCP8.5. In absolute terms, this means increases in JJA rainfall by up to 3-5 mm/day for RCP8.5. The decline of the South Asian monsoon for RCP8.5 after 2150 is due to a shift of the center of maximum precipitation out of the South Asian region towards South China. While the magnitude and timing of this shift must be viewed in the context of our intermediate-complexity model, observations suggest that a displacement of the center of precipitation may be possible under global warming (Wang et al., 2009). In all regions we find a strong quasi-linear correlation of monsoon rainfall with the regional temperature difference between land and ocean (Fig. 5d-f). Note that changes due to direct and indirect aerosol effects are not captured by simulations with CLIM*BER*-3α and may have significant influence on monsoon rainfall and circulation which is likely to counter-act that of global warming (Lau and Kim, 2006; Rosenfeld et al., 2008).

3.4 Steric sea level rise

Oceanic warming yields a steric sea level rise (SLR) of nearly 0.5 m for RCP8.5 by 2100 compared to the 1980-1999 average (Fig. 6). Thus, thermal oceanic expansion under RCP8.5 in our CLIM*BER*-3α simulations is about 20% higher than the upper 95% percentile (0.41 m by 2100) for the highest SRES scenario A1FI (see Table 10.7 in Meehl et al., 2007a) – in part because of slightly stronger anthropogenic forcing in RCP8.5. For RCP4.5 and RCP6, steric SLR is about 0.3 m by 2100 and thereby close to the upper 95% percentile provided in IPCC AR4 for the similar SRES B1 scenario. While for the upper three RCPs, steric SLR continues beyond 2500, the declining temperatures in RCP3-PD lead to a deceleration of steric SLR, a peaking at $\sim$0.3 m and a gradual reversal in the second half of the 23rd century, about 200 years after the peak in global temperatures. Other contributions to total sea level rise, in particular from melting of the Greenland and West Antarctic Ice Sheets, are beyond the scope of this study.

During an initial phase, we find a quasi-linear relationship between the rate of steric sea level rise and the global mean surface warming (Fig. 6, inset; cf. Rahmstorf, 2007). However, the quasi-linear relation fails as soon as global warming starts to decelerate, i.e. around 2100 for RCP8.5, and some time earlier for the lower scenarios. As suggested by Vermeer and Rahmstorf (2009), validity of semi-empirical pro-

jections of sea level change based on this relation might be extended by taking rapid adjustment processes into account.

The horizontal distribution of steric SLR, shown in Fig. 7 for RCP3-PD, is qualitatively similar under different scenarios. By 2100 (Fig. 7a), the weakening of the AMOC maximum (cf. Fig. 3a) and of the North Atlantic current produces a southeast-to-northwest SLR gradient in the North Atlantic via geostrophic adjustment (Levermann et al., 2005; Yin et al., 2010). Small shifts in the northern subpolar and subtropical gyre systems induce smaller-scale variations of SLR. The interhemispheric sea level pattern found by Levermann et al. (2005) for an AMOC shutdown is not reflected here because the AMOC change is largely confined to the North Atlantic; Southern Ocean outflow, i.e. the AMOC flux across 30°S, is only reduced by about 10% (not shown). By 2200, the AMOC has partly recovered, and the most prominent feature in the North Atlantic is a negative SLR anomaly (Fig. 7b) due to a 60% increase in the subpolar gyre (Fig. 3b; Häkkinen and Rhines, 2004; Levermann and Born, 2007). In the Southern Ocean, SLR patterns in 2200 are similar to those in 2100: A strengthening of the Antarctic Circumpolar Current above the level of no motion by about 4 Sv leads to below-average SLR around Antarctica (Fig. 7). On top of that, strengthening of the Ross and Weddell gyres by 5 Sv and 6 Sv, respectively, induces large horizontal SLR anomalies. Hattermann and Levermann (2010) found that a strengthening of those gyres may significantly enhance basal ice shelf melting around Antarctica.

Yin et al. (2010) showed by comparison of simulated and observed present-day dynamic sea level patterns in twelve IPCC AR4 AOGCMs that their ensemble mean performs better than any of the individual models. The SLR pattern found in our analysis is in good qualitative agreement with the ensemble mean projection of those models under the SRES A1B scenario (Yin et al., 2010).

3.5 Deep ocean warming

In contrast to the sea surface, deep ocean temperatures respond to atmospheric warming on centennial time scales. Due to its peaking characteristic, the RCP3-PD scenario is well suited to study the propagation of the warming signal into the deep ocean. Global average temperatures at 500 m and 1000 m depth exhibit delayed peaks around the years 2200 and 2300, respectively, compared to a surface warming peak in the middle of the 21st century (Fig. 8a). In the year 2370, about 300 years after the peak in global surface temperatures, major anomalies of up to 2°C are found in the upper 1000 m of the North Atlantic and Southern Ocean (Fig. 8b). In the North Atlantic, substantial warming is observed even below 2000 m depth. Despite the weakening of the AMOC noted earlier, the northern oceanic warming pattern clearly reflects the structure of the overturning cell.

In general, the strong deep oceanic warming signal results from outcropping of isopycnals (black lines in Fig. 8b) at high latitudes, i. e. a lack of density stratification, which is a characteristic and robust feature of the modern ocean circulation. Mixing along these surfaces of constant density is strongly enhanced compared to diapycnal mixing across these surfaces. In combination with the observed polar warming amplification, isopycnal mixing facilitates enhanced heat uptake as also observed in AOGCMs (e.g. Stouffer et al., 2006a) and is the reason for the observed deep ocean warming. These heat anomalies spread at intermediate depths around 500 m, with the effect that peak global-average warming at those depths exceeds that of the ocean surface (Fig. 8a). After surface temperatures have relaxed, oceanic heat uptake is reduced and, after 2300, the ocean eventually becomes a very weak heat source, further damping the decline of surface atmospheric temperatures (compare Fig. 9b). This weak heat exchange between ocean and atmosphere eventually cools deeper oceanic layers, but this cooling is so slow that the intermediate-depth warming persists for centuries even after surface temperatures have reached present-day levels of approximately 0.8°C relative to pre–industrial. Conversely, these oceanic heat anomalies serve as a long-term reservoir that slowly discharges into the atmosphere and delays surface cooling, as discussed in the following section.

4 Slow cooling under RCP3-PD

As mentioned in sec. 3.1, global cooling after the temperature peak in RCP3-PD is much slower, relative to the rate of GHG emissions, than the warming before the peak (Fig. 9a, blue line). We find that two processes are responsible for this asymmetry.

Generally oceanic heat uptake by vertical mixing creates thermal inertia that delays any temperature change at the surface (Fig. 9b). In order to identify additional effects, we isolate this ocean mixing effect with an intentionally simple energy-balance equation for global mean surface temperature anomaly $T(t)$, assuming a diffusive ocean (following Allen et al., 2009; Hansen et al., 1985):

$$a_1 \frac{dT}{dt} = a_3 log_2\left(\frac{C}{C_0}\right) - a_0 T - a_2 \int_0^t \frac{dT(t')}{dt'} \frac{dt'}{\sqrt{t-t'}} \qquad (1)$$

where $C(t)$ is CO_2 concentration; $C_0 = 280$ppm is the initial concentration at $t = 0$; a_1 is the heat capacity of the oceanic mixed layer; a_2 is ocean vertical diffusivity; $a_3 \simeq 1.3$°C is climate sensitivity not accounting for any feedbacks; and $1/a_0$ is the climate feedback factor, such that a_3/a_0 is the full climate sensitivity, which is ~ 3.4°C for CLIM*BER*-3α.

This model, with parameters a_{0-2} calibrated to match CLIM*BER*-3α, reproduces the global mean temperature simulated by CLIM*BER*-3α very well until about 2100 (black dashed line in Fig. 9a). However, at the beginning of the 22nd century, the CLIM*BER*-3α result deviates from the simple diffusive ocean heat uptake relationship: While the latter projects a steady cooling trend all the way until 2500,

CLIM*BER*-3α projects a substantial slow-down of the cooling around the year 2110 (vertical dashed line in Fig. 9). The cooling rate thereafter remains almost 50% lower than suggested by eq. (1) for about two centuries, consequently arriving at a significantly higher temperature. Plotted versus CO_2-equivalent GHG concentration, this is visible as a clear excursion from the smooth hysteresis projected according to eq. (1) (Fig. 10).

To test the robustness of this behaviour, we have conducted additional simulations using a set of scenarios that are identical to RCP3-PD until 2070. Thereafter, we set CO_2 emissions in RCP3-PD equal to zero or two, three, four or five times as large negative emissions as in the original RCP3-PD, respectively. Using these modified RCP3-PD scenarios, we then computed radiative forcings following the same process as in generating the recommended CMIP5 GHG concentrations of the RCPs (for details, see Meinshausen et al., submitted). Under all these modified RCP3-PD scenarios, CLIM*BER*-3α projects a drop in the cooling rate at the same time, near the year 2110, i.e., some decades after global mean temperature started to decline (thin grey lines in Fig. 9a). For zero emissions after 2070 (top grey line), this even leads to a slow global warming until the early 24$^{\text{th}}$ century, despite the net decrease in radiative forcing. Again, viewed relative to CO_2-equivalent GHG concentration, eq. (1) yields essentially the same hysteresis for all the scenarios (Fig. 10, dashed grey lines), while the CLIM*BER*-3α projections for the modified scenarios depart from that hysteresis soon after the peak (solid grey lines).

This result suggests that, on the one hand, the global mean temperature response of the coupled climate model to a peak-and-decline scenario such as RCP3-PD is, up until about 70 years after the peak in GHG concentrations, mainly governed by the heat capacity of the oceanic mixed layer and heat exchange with the deep ocean due to mixing. The inertia induced by these processes delays the cooling that results from the decline in GHG concentrations (Stouffer, 2004). On the other hand, another mechanism comes into play around the year 2110 that further reduces the cooling rate, over a period of two centuries, by almost 50%.

We find that a relatively rapid change in oceanic convection is responsible for this reduction. The depth of the wintertime oceanic mixed layer in the North Atlantic is a direct indicator of the strength of convection associated with the AMOC. This mixed layer depth shrinks during the warming phase in the 21$^{\text{st}}$ century, but then extends strongly between the years 2110 and 2150, which coincides with the change in the surface cooling rate (Fig. 9c). Enhanced convection in these latitudes results in enhanced heat loss of the ocean to the atmosphere; thus, globally, net ocean heat uptake is reduced by this effect (Fig. 9b, solid blue line), slowing down atmospheric cooling.

5 Discussion and conclusions

We have presented large-scale climatic consequences of the new RCP scenarios, which are designed for the forthcoming IPCC AR5 to span the full range of future pathways of anthropogenic GHG emissions currently discussed in the literature (Moss et al., 2008, page i). CLIM*BER*-3α atmospheric temperature projections and AOGCM emulations using MAGICC6 are qualitatively and quantitatively similar for the 21$^{\text{st}}$ century. CLIM*BER*-3α temperatures tend to be slightly higher than the median of the AOGCM emulations (cf. Fig. 1), owing to the difference in climate sensitivity. While the CLIM*BER*-3α simulations are based on the standard settings presented in Montoya et al. (2005), the wider range of possible climate responses is covered by the emulation ensemble with MAGICC6, spanning climate sensitivities from 1.9°C (emulation of the NCAR PCM model) to 5.7°C (emulation of the MIROC3.2 high resolution model, see Meinshausen et al., 2008, Table 4). With respect to atmospheric quantities, the coarse resolution of CLIM*BER*-3α and the limitations of the statistical-dynamical representation must be kept in mind. On the other hand, large-scale oceanic quantities have been shown to be in good agreement with recent AOGCM results.

Our evaluation of the peak-and-decline scenario RCP3-PD reveals that global maximal temperatures can be expected close to 1.5°C warming relative to pre–industrial levels. Owing to negative CO_2 emissions, concentrations under this scenario are projected to drop markedly after peaking in 2070, and induce a slow cooling. This finding is consistent with recent studies using other models of varying complexity (e.g. Solomon et al., 2009), which showed that under zero-emission scenarios temperatures are projected not to drop substantially for several centuries. Our work goes beyond those studies by demonstrating that in a physical climate model, cooling is not only delayed by mixing-related heat exchange with the ocean, but that dynamical effects can significantly add to the delay. The abrupt strengthening of convection in the North Atlantic indicates an important role of internal dynamical processes in the oceans, especially because the timing of the convection change seems to be independent of the rate of (negative) GHG emissions, once atmospheric temperatures have started to fall. Although the exact timing will probably differ across models, the onset of strong convection is likely to be a robust feature, because declining atmospheric temperatures lead to stronger cooling of surface waters and thus reduce the stability of the water column.

The projections of steric sea level rise presented here are generally consistent with previous simulations. The highest scenario, RCP8.5, being warmer than the highest SRES scenario, yields enhanced steric sea level rise of up to 2 m by 2500. According to our simulations, thermal oceanic expansion can be halted only for emission trajectories corresponding to, or below, RCP3-PD. In this scenario we observe an enhanced oceanic warming of intermediate depth due to

polar amplification in combination with the lack of oceanic density stratification in high latitudes. The associated heat content persists for centuries. Thus, these results will allow future studies to quantify the risk of such a mid-ocean warming for marine ecosystems (Sarmiento et al., 2004) and environments. For example, prolonged deep ocean warming could be sufficient to trigger the dissociation of shallow methane hydrates trapped in ocean sediments, and thereby release additional amounts of greenhouse gases into the atmosphere (Reagan and Moridis, 2008; Archer et al., 2009). Furthermore, melting of Antarctic ice shelves (Holland et al., 2008) and the initiation of oceanic anoxic events (Hofmann and Schellnhuber, 2009; Stramma et al., 2009) could be facilitated.

Acknowledgements. This work was supported by the Heinrich Böll Foundation, the German National Academic Foundation, and the BMBF PROGRESS project. MM received support from the UFOPLAN project FKZ 370841103 by the German Federal Environment Agency. NCEP Reanalysis Derived data was provided by the NOAA/OAR/ESRL PSD, Boulder, Colorado, USA, from their Web site at http://www.esrl.noaa.gov/psd/. We thank two anonymous referees for their helpful comments.

References

Allen, M. R., Frame, D. J., Huntingford, C., Jones, C. D., Lowe, J. A., Meinshausen, M., and Meinshausen, N.: Warming caused by cumulative carbon emissions towards the trillionth tonne, Nature, 458, 1163–1166, doi:10.1038/nature08019, 2009.

Archer, D., Buffett, B., and Brovkin, V.: Ocean methane hydrates as a slow tipping point in the global carbon cycle, Proc. Natl. Acad. Sci. U.S.A., 106, 20 596–20 601, doi:10.1073/pnas.0800885105, 2009.

Brohan, P., Kennedy, J., Harris, I., Tett, S., and Jones, P.: Uncertainty estimates in regional and global observed temperature changes: A new data set from 1850, Journal of Geophysical Research - Atmosphere, 111, doi:10.1029/2005JD006548, 2006.

Clarke, L., Edmonds, J., Jacoby, H., Pitcher, H., Reilly, J., and Richels, R.: Scenarios of Greenhouse Gas Emissions and Atmospheric Concentrations. Sub-report 2.1A of Synthesis and Assessment Product 2.1 by the U.S. Climate Change Science Program and the Subcommittee on Global Change Research, U.S. Department of Energy, p. 154, 2007.

Fichefet, T. and Maqueda, M. A. M.: Sensitivity of a global sea ice model to the treatment of ice thermodynamics and dynamics, Journal of Geophysical Research, 102, 12 609–12 646, 1997.

Fujino, J., Nair, R., Kainuma, M., Masui, T., and Matsuoka, Y.: Multi-gas Mitigation Analysis on Stabilization Scenarios Using Aim Global Model, The Energy Journal, 0, 343–354, 2006.

Gregory, J. M., Dixon, K. W., Stouffer, R. J., Weaver, A. J., Driesschaert, E., Eby, M., Fichefet, T., Hasumi, H., Hu, A., Jungclaus, J. H., Kamenkovich, I. V., Levermann, A., Montoya, M., Murakami, S., Nawrath, S., Oka, A., Sokolov, A. P., and Thorpe, R. B.: A model intercomparison of changes in the Atlantic thermohaline circulation in response to increasing atmospheric CO_2 concentration, Geophysical Research Letters, 32, doi:10.1029/2005GL023209, 2005.

Häkkinen, S. and Rhines, P. B.: Decline of Subpolar North Atlantic Circulation During the 1990s, Science, 304, 555–559, 2004.

Hansen, J., Russell, G., Lacis, A., Fung, I., Rind, D., and Stone, P.: Climate response-times - dependence on climate sensitivity and ocean mixing, Science, 229, 857–859, 1985.

Hattermann, T. and Levermann, A.: Response of Southern Ocean circulation to global warming may enhance basal ice shelf melting around Antarctica, Climate Dynamics, doi:10.1007/s00382-009-0643-3, 2010.

Hofmann, M. and Schellnhuber, H.-J.: Oceanic acidification affects marine carbon pump and triggers extended marine oxygen holes, Proc. Natl. Acad. Sci. U.S.A., 106, 3017–3022, doi:10.1073/pnas.0813384106, 2009.

Holland, P. R., Jenkins, A., and Holland, D. M.: The response of ice shelf basal melting to variations in ocean temperature, Journal of Climate, 21, 2558–2572, doi:10.1175/2007JCLI1909.1, 2008.

Kistler, R., Kalnay, E., Saha, S., White, G., Woollen, J., Chelliah, M., Ebisuzaki, W., Kanamitsu, M., Kousky, V., van den Dool, H., Jenne, R., and Fiorino, M.: The NCEP/NCAR 50-year reanalysis, Bull. Amer. Meteor. Soc., 82, 247 – 267, 2001.

Kripalani, R. H., Oh, J. H., and Chaudhari, H. S.: Response of the East Asian summer monsoon to doubled atmospheric CO2: Coupled climate model simulations and projections under IPCC AR4, Theor. Appl. Climatol., 87, 1–28, doi:10.1007/s00704-006-0238-4, 2007.

Lau, K. M. and Kim, K. M.: Observational relationships between aerosol and Asian monsoon rainfall, and circulation, Geophysical Research Letters, 33, doi:10.1029/2006GL027546, 2006.

Levermann, A. and Born, A.: Bistability of the subpolar gyre in a coarse resolution climate model, Geophysical Research Letters, 34, doi:10.1029/2007GL031732, 2007.

Levermann, A., Griesel, A., Hofmann, M., Montoya, M., and Rahmstorf, S.: Dynamic sea level changes following changes in the thermohaline circulation, Climate Dynamics, 24, 347–354, 2005.

Levermann, A., Mignot, J., Nawrath, S., and Rahmstorf, S.: The role of northern sea ice cover for the weakening of the thermohaline circulation under global warming, Journal of Climate, 20, 4160–4171, 2007.

May, W.: Climatic changes associated with a global "2 degrees C-stabilization" scenario simulated by the ECHAM5/MPI-OM coupled climate model, Climate Dynamics, 31, 283–313, doi:10.1007/s00382-007-0352-8, 2008.

Meehl, G. A., Stocker, T. F., Collins, W. D., Friedlingstein, P., Gaye, A. T., Gregory, J. M., Kitoh, A., Knutti, R., Murphy, J. M., Noda, A., Raper, S. C. B., Watterson, I. G., Weaver, A. J., and Zhao, Z.-C.: Climate Change 2007: The Physical Science Basis. Contribution of Working Group I to the Fourth Assessment Report of the Intergovernmental Panel on Climate Change, chap. Global Climate Projections, Cambridge University Press, Cambridge, United Kingdom and New York, NY, USA, 2007a.

Meehl, G. A., Stocker, T. F., Collins, W. D., Friedlingstein, P., Gaye, A. T., Gregory, J. M., Kitoh, A., Knutti, R., Murphy, J. M., Noda, A., Raper, S. C. B., Watterson, I. G., Weaver, A. J., and Zhao, Z.-C.: Climate Change 2007: The Physical Science Basis. Contribution of Working Group I to theFourth Assessment Report of the Intergovernmental Panel on Climate Change, chap. Climate Models and their Evaluation, Cambridge University Press, Cambridge, United Kingdom and New York, NY, USA, 2007b.

Meinshausen, M., Raper, S. C. B., and Wigley, T. M. L.: Emulating IPCC AR4 atmosphere-ocean and carbon cycle models for projecting global-mean, hemispheric and land/ocean temperatures: MAGICC 6.0., Atmos. Chem. Phys. Discuss., 8, 6153–6272, 2008.

Meinshausen, M., Smith, S., Calvin, K., Daniel, J. S., Kainuma, M., Lamarque, J.-F., Matsumoto, K., Montzka, S. A., Raper, S. C. B., Riahi, K., Thomson, A. M., Velders, G. J. M., and van Vuuren, D.: The RCP Greenhouse Gas Concentrations and their Extension from 1765 to 2300, Climatic Change, http://www.pik-potsdam.de/~mmalte/pubs/09_GHG_Concentrations&Extension_1Sep2010.pdf, submitted.

Mignot, J., Levermann, A., and Griesel, A.: A decomposition of the Atlantic Meridional Overturning Circulation into physical components using its sensitivity to vertical diffusivity, Journal of Physical Oceanography, 36, 636–650, 2006.

Montoya, M. and Levermann, A.: Surface wind-stress threshold for glacial Atlantic overturning, Geophysical Research Letters, 35, doi:10.1029/2007GL032560, 2008.

Montoya, M., Griesel, A., Levermann, A., Mignot, J., Hofmann, M., Ganopolski, A., and Rahmstorf, S.: The Earth System Model of Intermediate Complexity CLIM*BER*-3α. Part I: description and performance for present day conditions, Climate Dynamics, 25, 237–263, 2005.

Moss, R., Babiker, M., Brinkman, S., Calvo, E., Carter, T., Edmonds, J., Elgizouli, I., Emori, S., Erda, L., Hibbard, K., Jones, R., Kainuma, M., Kelleher, J., Lamarque, J. F., Manning, M., Matthews, B., Meehl, J., Meyer, L., Mitchell, J., Nakicenovic, N., ONeill, B., Pichs, R., Riahi, K., Rose, S., Runci, P., Stouffer, R., van Vuuren, D., Weyant, J., Wilbanks, T., van Ypersele, J. P., and Zurek, M.: Towards New Scenarios for Analysis of Emissions, Climate Change, Impacts, and Response Strategies, http://www.ipcc.ch/pdf/supporting-material/expert-meeting-report-scenarios.pdf, 2008.

Moss, R., Edmonds, J., Hibbard, K., Manning, M. R., Rose, S., van Vuuren, D., Carter, T., Emori, S., Kainuma, M., Kram, T., Meehl, G., Mitchell, J., Nakicenovic, N., Riahi, K., Smith, S., Stouffer, R., Thomson, A., Weyant, J., and Wilbanks, T.: The next generation of scenarios for climate change research and assessment, Nature, 463, 747–756, doi:10.1038/nature08823, 2010.

Nakicenovic, N. and Swart, R., eds.: IPCC Special Report on Emissions Scenarios, Cambridge University Press, 2000.

Pacanowski, R. C. and Griffies, S. M.: The MOM-3 manual, Tech. Rep. Tech. Rep. 4, NOAA/Geophyical Fluid Dynamics Laboratory, Princeton, NJ, USA, 1999.

Petoukhov, V., Ganopolski, A., Brovkin, V., Claussen, M., Eliseev, A., Kubatzki, C., and Rahmstorf, S.: CLIMBER-2: a climate system model of intermediate complexity. Part I: model description and performance for present climate, Climate Dynamics, 16, 1, 2000.

Rahmstorf, S.: A Semi-Empirical Approach to Projecting Future Sea-Level Rise, Science, 315, 368–370, doi:10.1126/science.1135456, 2007.

Reagan, M. T. and Moridis, G. J.: Dynamic response of oceanic hydrate deposits to ocean temperature change, Journal of Geophysical Research - Oceans, 113, doi:10.1029/2008JC004938, 2008.

Riahi, K., Gruebler, A., and Nakicenovic, N.: Scenarios of long-term socio-economic and environmental development under climate stabilization, Technological Forecasting and Social Change, 74, 887 – 935, doi:10.1016/j.techfore.2006.05.026, 2007.

Rosenfeld, D., Lohmann, U., Raga, G. B., O'Dowd, C. D., Kulmala, M., Fuzzi, S., Reissell, A., and Andreae, M. O.: Flood or drought: How do aerosols affect precipitation?, Science, 321, 1309–1313, doi:10.1126/science.1160606, 2008.

Sarmiento, J., Slater, R., Barber, R., Bopp, L., Doney, S., Hirst, A., Kleypas, J., Matear, R., Mikolajewicz, U., Monfray, P., Soldatov, V., Spall, S., and Stouffer, R.: Response of ocean ecosystems to climate warming, Global Biogeochemical Cycles, 18, doi:10.1029/2003GB002134, 2004.

Schewe, J. and Levermann, A.: The role of meridional density differences for a wind-driven overturning circulation, Climate Dynamics, 34, 547–556, doi:10.1007/s00382-009-0572-1, 2010.

Smith, S. J. and Wigley, T. M. L.: Multi-gas forcing stabilization with Minicam, Energy Journal, pp. 373–391, 2006.

Solomon, S., Plattner, G.-K., Knutti, R., and Friedlingstein, P.: Irreversible climate change due to carbon dioxide emissions, Proc. Natl. Acad. Sci. U.S.A., 106, 1704–1709, doi:10.1073/pnas.0812721106, 2009.

Stouffer, R.: Time scales of climate response, Journal of Climate, 17, 209–217, 2004.

Stouffer, R., Broccoli, A., Delworth, T., Dixon, K., Gudgel, R., Held, I., Hemler, R., Knutson, T., Lee, H., Schwarzkopf, M., Soden, B., Spelman, M., Winton, M., and Zeng, F.: GFDL's CM2 global coupled climate models. Part IV: Idealized climate response, Journal of Climate, 19, 723–740, 2006a.

Stouffer, R. J., Yin, J., Gregory, J. M., Dixon, K. W., Spelman, M. J., Hurlin, W., Weaver, A. J., Eby, M., Flato, G. M., Hasumi, H., Hu, A., Jungclaus, J. H., Kamenkovich, I. V., Levermann, A., Montoya, M., Murakami, S., Nawrath, S., Oka, A., Peltier, W. R., Robitaille, D. Y., Sokolov, A. P., Vettoretti, G., and Weber, S. L.: Investigating the Causes of the Response of the Thermohaline Circulation to Past and Future Climate Changes, Journal of Climate, 19, 1365–1387, 2006b.

Stramma, L., Visbeck, M., Brandt, P., Tanhua, T., and Wallace, D.: Deoxygenation in the oxygen minimum zone of the eastern tropical North Atlantic, Geophysical Research Letters, 36, doi:10.1029/2009GL039593, 2009.

Trenberth, K., Olson, J., and Large, W.: A Global Ocean Wind Stress Climatology based on ECMWF Analyses, Tech. Rep. NCAR/TN-338+STR, National Center for Atmospheric Research, Boulder, Colorado, USA, 1989.

Trenberth, K., Jones, P., Ambenje, P., Bojariu, R., Easterling, D., Tank, A. K., Parker, D., Rahimzadeh, F., Renwick, J., Rusticucci, M., Soden, B., and Zhai, P.: Climate Change 2007: The Physical Science Basis. Contribution of Working Group I to the Fourth Assessment Report of the Intergovernmental Panel on Climate Change, chap. Observations: Surface and Atmospheric Climate Change, Cambridge University Press, Cambridge, United Kingdom and New York, NY, USA, 2007.

van Vuuren, D. P., Den Elzen, M. G. J., Lucas, P. L., Eickhout, B., Strengers, B. J., van Ruijven, B., Wonink, S., and van Houdt, R.: Stabilizing greenhouse gas concentrations at low levels: an assessment of reduction strategies and costs, Climatic Change, 81, 119–159, doi:10.1007/s10584-006-9172-9, 2007.

Vermeer, M. and Rahmstorf, S.: Global sea level linked to global temperature, Proc. Natl. Acad. Sci. U.S.A., 106, 21 527–21 532, doi:10.1073/pnas.0907765106, 2009.

Wang, C., Kim, D., Ekman, A. M. L., Barth, M. C., and Rasch, P. J.: Impact of anthropogenic aerosols on Indian summer monsoon, Geophysical Research Letters, 36, doi:10.1029/2009GL040114, 2009.

Washington, W. M., Knutti, R., Meehl, G. A., Teng, H., Tebaldi, C., Lawrence, D., Buja, L., and Strand, W. G.: How much climate change can be avoided by mitigation?, Geophysical Research Letters, 36, doi:10.1029/2008GL037074, 2009.

Wigley, T. M. L. and Raper, S. C. B.: Interpretation of high projections for global-mean warming, Science, 293, 451–454, doi: 10.1126/science.1061604, 2001.

Winton, M.: Amplified Arctic climate change: What does surface albedo feedback have to do with it?, Geophysical Research Letters, 33, doi:10.1029/2005GL025244, 2006.

Wise, M., Calvin, K., Thomson, A., Clarke, L., Bond-Lamberty, B., Sands, R., Smith, S. J., Janetos, A., and Edmonds, J.: Implications of Limiting CO2 Concentrations for Land Use and Energy, Science, 324, 1183–1186, doi:10.1126/science.1168475, 2009.

Wu, P., Wood, R., Ridley, J., and Lowe, J.: Temporary acceleration of the hydrological cycle in response to a CO2 rampdown, Geophysical Research Letters, 37, L12 705, doi:10.1029/2010GL043730, 2010.

Yin, J., Griffies, S. M., and Stouffer, R. J.: Spatial Variability of Sea Level Rise in Twenty-First Century Projections, Journal of Climate, 23, 4585–4607, doi:10.1175/2010JCLI3533.1, 2010.

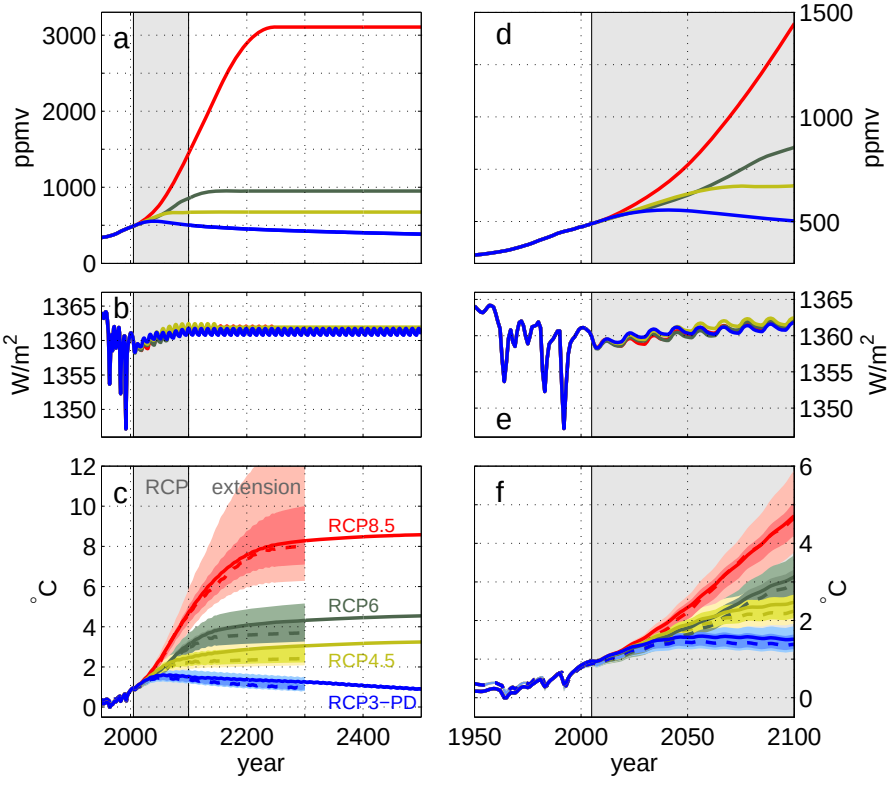

Fig. 1. Forcing and global mean temperature response of the CLIM*BER*-3α climate model under the RCP3-PD (blue), RCP4.5 (yellow), RCP6 (grey) and RCP8.5 (red) scenarios and their extensions until 2500. The grey vertical band marks the RCP period 2005 to 2100. (a) CO_2-equivalence concentration (in ppmv) of longwave absorbers (Kyoto and Montreal protocol greenhouse gases as well as tropospheric ozone). (b) Incoming solar irradiance (W/m^2), modified by the radiative forcing of agents active in the shortwave range (mainly volcanic and anthropogenic aerosols) and changes in surface albedo due to land-use change. (c) Global surface air temperature (SAT) difference in °C compared to pre–industrial (Brohan et al., 2006), for the CLIM*BER*-3α simulations (solid lines) and 19 AOGCM emulations using MAGICC6 (the dashed line denotes the median, and dark and light shading denotes the 50% and 80% range, respectively). (d) to (f): As (a) to (c), but enlarged for the period 1950-2100.

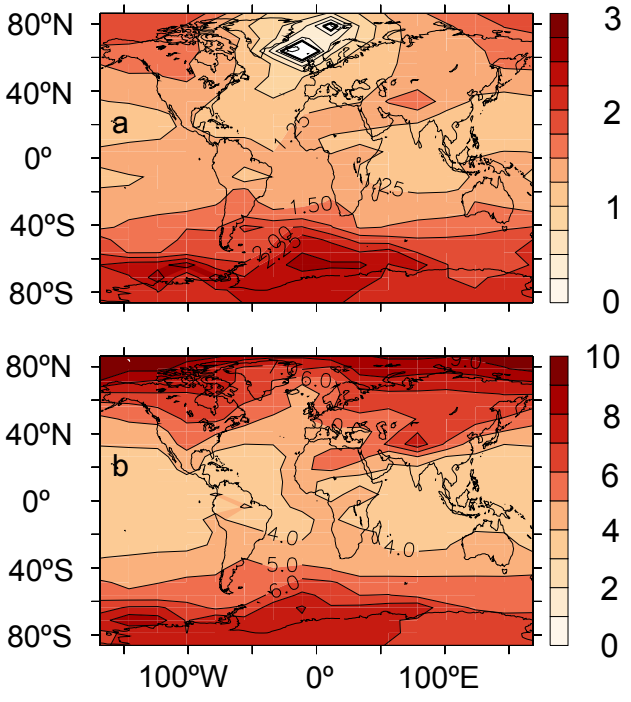

Fig. 2. (a) Surface air temperature anomaly for the year 2100, in °C, for RCP3-PD. Average warming south of 60°S is 1.60 times higher than the global mean. Average warming north of 60°N is only 0.83 times the global mean (1.4°C), because the cooling effect of a reduction in the Atlantic Meridional Overturning Circulation (AMOC) counteracts polar amplification. (b) Same for RCP8.5 (with a global mean of 4.8°C). The polar amplification factors are 1.48 in the south and 1.53 in the north.

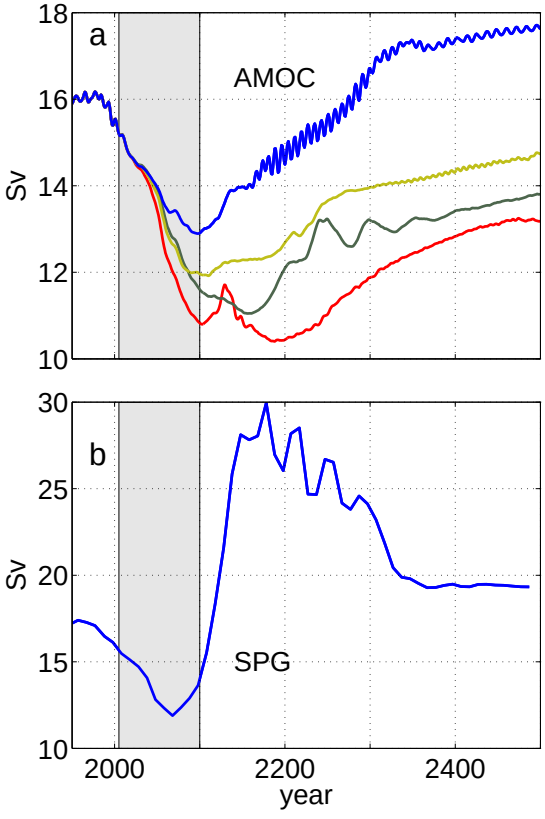

Fig. 3. (a) Maximum AMOC strength of the Atlantic Meridional Overturning Circulation (AMOC) in Sv ($10^6 m^3 s^{-1}$), for RCP3-PD (blue), RCP4.5 (yellow), RCP6 (grey), and RCP8.5 (red). (b) North Atlantic subpolar gyre strength, in Sv, computed from meridional velocities at 55°N between 33.8°W and the Labrador coast (62°W).

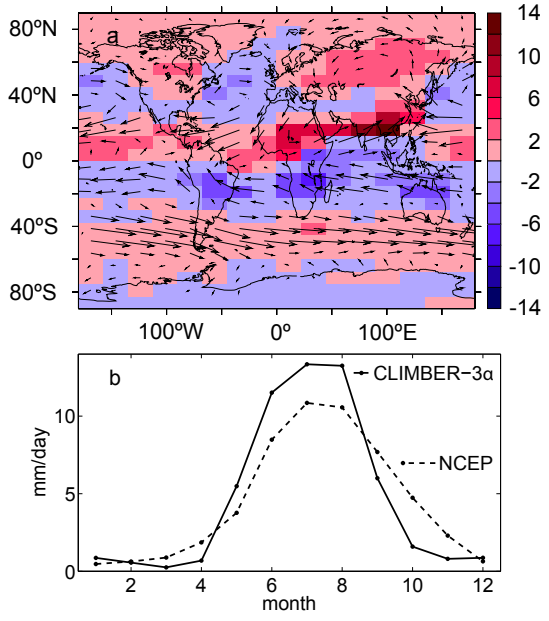

Fig. 4. (a) Difference between average boreal summer (JJA) and winter (DJF) precipitation (shading, in mm/day), and average summer (JJA) near-surface winds (vectors) in the control (pre–industrial) climate of CLIM*BER*-3α. (b) Seasonal cycle of monthly average precipitation in the South Asian monsoon region in CLIM*BER*-3α's control climate (solid line) and in the NCEP-NCAR reanalysis (Kistler et al., 2001), averaged over the period 1948-2007 (dashed line).

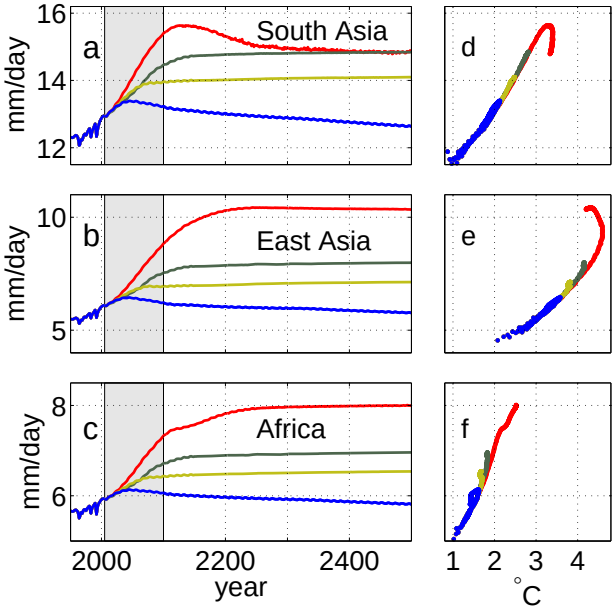

Fig. 5. Average seasonal (JJA) precipitation of (a) South Asian (67.5-112.5°E, 15-22.5°N), (b) East Asian (90-135°E, 22.5-37.5°N), and (c) African (22.5°W-22.5°E, 0-15°N) summer monsoon (mm/day). Panels (d-f) show the respective regional monsoon precipitation versus the difference in JJA regional surface air temperature over land and the adjacent ocean. Generally this relation shows a clear linear trend. A shift of precipitation from the south Asian monsoon region towards the east Asian region leads to deviations for strong warming and does not represent a qualitative change in this relation.

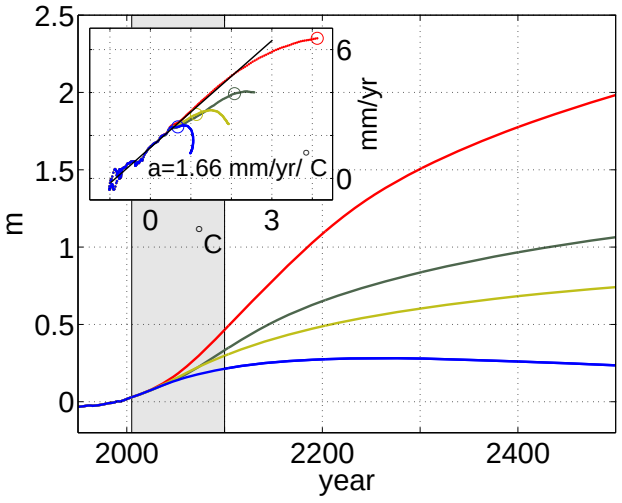

Fig. 6. Globally averaged steric sea level change (in m) relative to 1980-1999, under the RCP3-PD (blue), RCP4.5 (yellow), RCP6 (grey) and RCP8.5 (red) scenarios and their extensions in CLIM*BER*-3α. The inset shows the rate of steric sea level rise (in mm/yr, smoothed with a 15-year moving average) between 1800 and 2100 as a function of global surface warming above the 1980-1999 mean (in °C). The slope of the quasi-linear part is 1.66 mm yr^{-1} °C^{-1} (black line; cf. Rahmstorf, 2007). Circles mark the timing of peak GHG emissions.

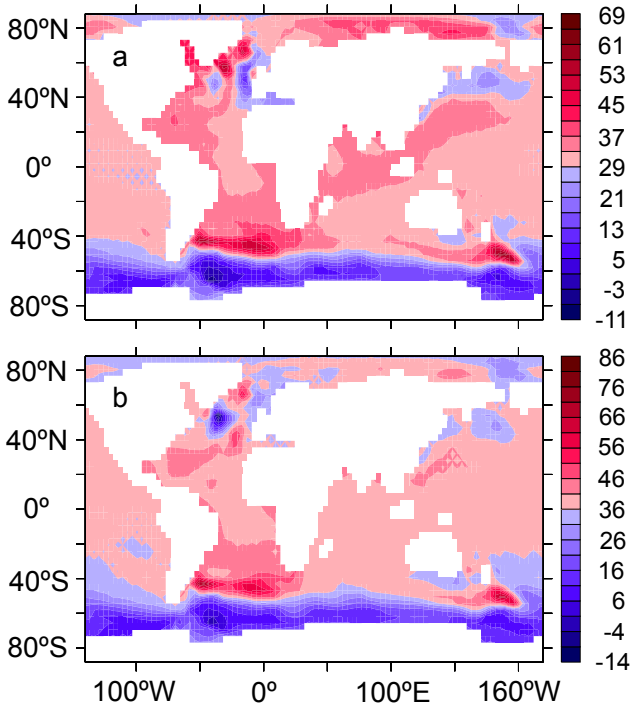

Fig. 7. Horizontal pattern of steric sea level change (in cm), relative to pre–industrial, under RCP3-PD: (a) Year 2100, (b) year 2200. The shading emphasizes the anomalies relative to the global average steric SLR (about 29 cm in 2100 and 36 cm in 2200).

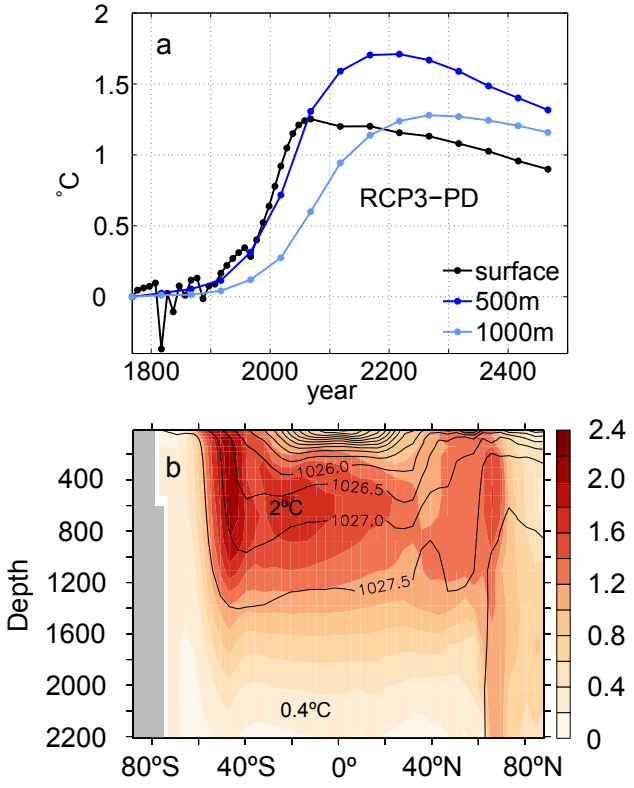

Fig. 8. Ocean response to the RCP3-PD scenario: (a) Global average ocean temperature difference relative to pre–industrial levels, at the ocean surface (black) and at 500 m (dark blue) and 1000 m (light blue) depth. Due to polar amplification and outcropping oceanic isopycnals at high latitudes, peak warming is stronger at intermediate depth around 500 m than at the surface. (b) Zonal average ocean warming in the year 2370, compared to pre–industrial levels (shading, in °C; ocean depth in m). Overlaid are contours of constant density (isopycnals; in kg/m^3).

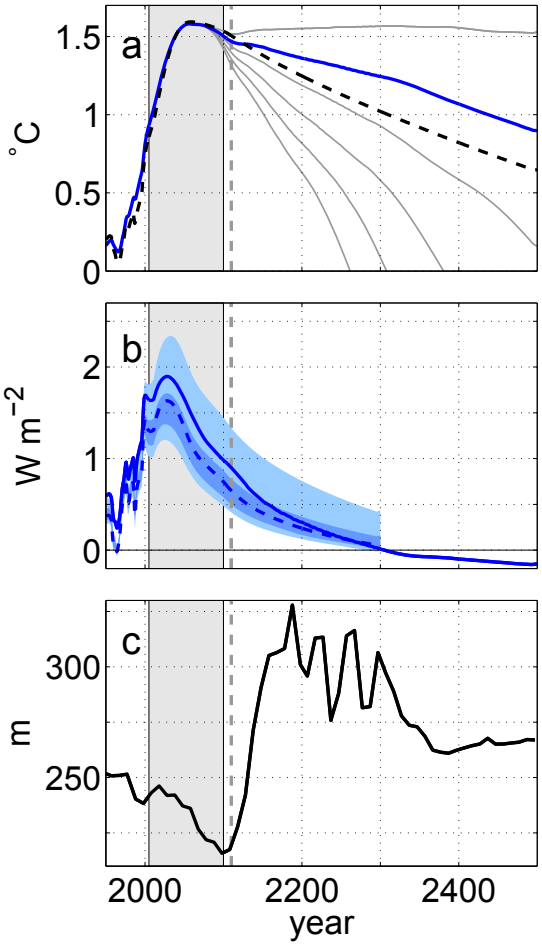

Fig. 9. Slow-down of global cooling under the RCP3-PD scenario: (a) Global surface air temperature anomaly as in Fig. 1c (blue line), compared to the result of the simple energy-balance equation (1) that only takes into account diffusive oceanic mixing (dashed black line). Thin grey lines represent modified scenarios that are identical to RCP3-PD until 2070, and after that have zero emissions or two, three, four or five times as large negative emissions as RCP3-PD, respectively. All curves are smoothed with an 11-year running mean to remove short-term variability from solar and volcanic sources. The vertical dashed line marks the year 2110. (b) Globally averaged heat flux from atmosphere to ocean. Increasing GHG concentration results in enhanced oceanic heat uptake which declines after the peak in atmospheric warming and vanishes around the year 2300 after which the ocean becomes a source for atmospheric warming. The solid line is the CLIM*BER*-3α simulation, while the 19 AOGCM emulations using MAGICC6 are represented by the dashed line (median) and shading (50% and 80% range). The onset of convection in the southern North Atlantic appears here as a distinct drop in ocean heat uptake after 2110 (vertical dashed line). All curves are smoothed as in (a). (c) Average depth of the North Atlantic ocean mixed layer in winter (January-April) south of the latitudes of Iceland (40°W-0°, 50-65°N). Starting around the year 2110 (vertical dashed line), an abrupt increase in mixed layer depth marks the onset of enhanced convection.

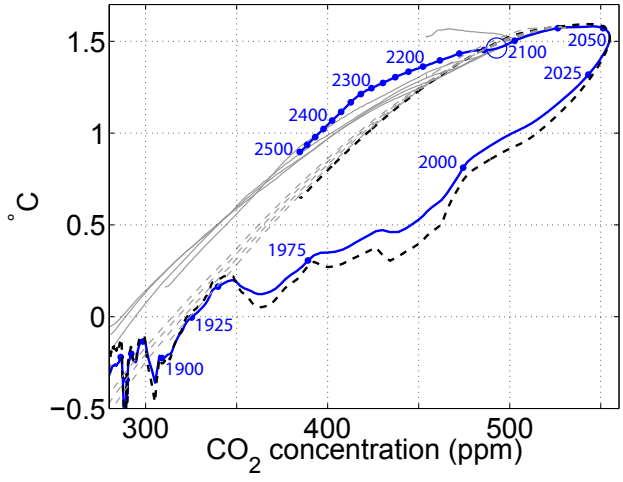

Fig. 10. As Fig. 9a, but plotted versus CO_2-equivalence concentration (sum of longwave absorbers) instead of time, and with the results of eq. (1) for the modified scenarios shown as dashed grey lines. This figure represents the transient "hysteresis" of global warming in RCP3-PD (blue line, marked every 25 years) and the modified peak-and-decline scenarios, i.e. how much GHG reduction it takes to cool the surface back to a given temperature that it had during the warming phase. The dashed lines show the hysteresis expected from the processes represented by eq. (1), while the solid lines show the hysteresis behaviour observed in CLIM*BER*-3α. The convection-related slow-down of the cooling rate (marked by a blue circle for the RCP3-PD scenario) translates into a widening of the hysteresis. The slow-down occurs at the same time under different scenarios (at the beginning of the 21st century, see thin grey lines in Fig. 9a), and at different CO_2 concentrations.